Journal of Chemical Technology and Metallurgy, 48, 3, 2013, 296-307

OPTIMIZATION OF THE BASIC PARAMETERS OF CATHODIC DEPOSITION OF Ce-CONVERSION COATINGS ON D16 AM CLAD ALLOY

S. Kozhukharov[1], J.A.P. Ayuso[2], D.S. Rodríguez[2], O.F. Acuña[2],
M. Machkova[1], V. Kozhukharov[1]

[1] *University of Chemical Technology and Metallurgy*
8 Kl. Ohridski, 1756 Sofia, Bulgaria
E-mail:stephko1980@abv.bg
[2] *University of Vigo, Lagoas,*
Marcosende 36310 (Spain)

Received 18 March 2013
Accepted 05 May 2013

ABSTRACT

The present research work is investigation on the probabilities for application of a new cerium compound, for cathodic electrodeposition of cerium based conversion coatings (CeCC) for protection of D16 AM alloy against corrosion. For the purpose of the present study, diammonium pentanitrocerate $(NH_4)_2Ce(NO_3)_5$ was used, where the cerium is represented in the anionic moiety, instead of the electrolytes used up to nowadays. The barrier ability and durability against corrosion of all coatings were evaluated by electrochemical methods – Linear Sweep Voltammetry (LSV) and Electrochemical Impedance Spectroscopy (EIS). Additionally, selected specimens underwent morphological characterization by means of canning Electronic Microscopy (SEM) combined with Energy Dispersive X-ray spectroscopy (EDX). As a result, various parameters and conditions of deposition, such as the preliminary treatment, concentration of the basic substance and additives, density of the applied electric current and duration of deposition were elucidated.

Keywords: corrosion protection, aluminium alloy CeCC, EIS, LSV, SEM and EDS.

INTRODUCTION

Regardless the employment of entire generations of new materials as carbon fibres and various composites in the transport and especially in the aircraft industry, the aluminium alloys still remain the basic constructive materials. Especially, AA2024 and AA7075 alloys are objects of special attention, due to their remarkable mechanical strength [1], being the basic constructional material for commercial [2] and military [3 - 5] aircraft. In the former case, the aluminium fuselages render "visibility" for the aircraft and airport radars, whereas in the military air-transport, the Al-frames shield the on-board navigation and communication equipment, against exterior electromagnetic influence. Recently, the importance of these alloys increased, due to their capabilities to be employed in the automobile industry [6 - 8]. In addition, the aluminium alloys encountered application in the marine industry for production of sport boats and even ships [9 - 11]. The main advantage of the aluminium alloys, compared to the steels is that the former are much lighter (about 2.723 tonnes/m^3) than the latter (about 7.840 tonnes/ m^3) [12]. Finally, the aluminium alloys are valuable for military naval building, rendering to the ships lower radar detection visibility [13], compared to the steel constructions.

Nevertheless, the corrosion protection by coatings is indispensable for all kinds of aluminium details and equipment. The conventional coatings are always composed by multilayer systems, where each layer has its own function [14-17]. On the other hand, the environmental restrictions regarding the employment of chromium and other heavy metals in EC [18, 19] and USA [20, 21] impose demants for alaboration of environmentally acceptable coatings. In that means, the Ce(III) compounds have proven to be excellent

inhibitors for localised, particularly pitting corrosion, whereas the Ce(IV) species act rather as corrosion activators [22-24]. The importance of the anionic part of the Ce-compounds has also been described, elsewhere [25]. All the facts mentioned above predetermine the nowadays elevated interest to the application of Ce oxides/hydroxides in form of Cerium containing primary coating layers on aluminium alloys [3, 4, 26-34] and stainless steel [37 - 40].

Arenas et al. [31] define the conversion coatings as products of chemical or electrochemical process, consisted on formation of a metallic oxide, with different properties, being substitute of the native superficial oxide layer of the respective substrate. Consequently, CeCC could be deposited by various methods, such as spontaneous deposition [3, 4, 26, 27, 30], spray coating [34] electrodeposition [35], spin coating, [41], etc.

EXPERIMENTAL

Composition and of the metallic substrates

All substrates were composed of aluminium alloy, D16-AM, described in GOST 172342 – 99. According to [42], this alloy is typical presenter of the AA2024 class. The alloy sheet for the present work is produced in Ukraine, and delivered by Klöckner Metalsnab AD, (Bulgaria) [43]. Because the standards allow some deviations from the basic nominal composition, the Al-sheet was submitted to an additional analysis, in order to determine its exact chemical composition. The element determination was performed by Inductively Coupled Plasma Optical Emission Spectroscopy (ICP-OES) in the Central Scientific Research Laboratory "Geokhimia"- Sofia. The exact composition of the alloy is summarized in Table 1.

The alloy sheet was cut to metallic coupons with size dimensions, shown in Fig. 1. Afterwards, they were subsequently polished up to 1000 grits emery paper, etched in NaOH solution (50 g/l) at 55°C for 5 minutes, and activated in diluted HNO_3 (1:1) for 5 minutes, at ambient temperature. Before each stage of the procedure, the samples passed cleaning by vigorous tap-water, followed by distilled water cleaning.

Coating deposition

The CeCCs were deposited via electrodeposition at either -2, or -5 mA/cm^2, for 5 min from water solutions of $(NH_4)_2Ce(NO_3)_5.4.H_2O$ – ("Alfa Aesar", Karlsruhe, Germany) with concentrations, varying from 0.03 to 0.10 M. Prior the respective electrodeposition, 30 % H_2O_2 ("Valerus", Sofia, Bulgaria) was added to the solutions, in 1 to 10 ml. additions to 100 ml. of CeCC deposition solution. This approach enabled to determine the optimal composition of the coating solution.

Measurements and characterizations

The electrochemical CeCC depositions were performed in a Galvanostatic regime, allowing recording of the potential during coating deposition and the following of its kinetics. Afterwards, the CeCC corrosion protective properties were characterized by linear sweep voltammetry and electrochemical impedance spectroscopy. Both the depositions and characterizations were performed in three electrode "flat cell", according to ISO 16773-2:2007 (E) Standard [44]. In both cells, Ag/AgCl-3M KCl, commercial electrode, model 6.0733.100, product of Metrohm (Netherlands) served as reference. The original "horseshoe" – shaped counter electrode was used for the needs of electrodeposition, whereas cylinder-shaped platinum net with highly developed superficial area was used for counter electrode in the test procedures. Other differences between the deposition and test cell, were the areas of the samples exposed to the liquid medium (shown in Fig. 1(c)), as well as its composition. The corrosion protective properties of CeCC, were examined after 24 h of exposition to naturally aerated 3.5% NaCl model corrosive medium. This exposure extension was selected, since in previous works [45, 46] was established that the Open Circuit Potential (OCP) stabilizes its value after at least 8 – 9 hours of exposition. The specimens were not submitted to larger exposition extensions, because the anodic polarization

Table 1. Composition of AA2024 alloy according to ICP – OES analysis.

Element	Al	Cu	Fe	Mg	Mn	Ni	Si
Content ($\%_{wt.}$)	Residual	3.716	0.404	1.259	0.537	0.055	< 0.01

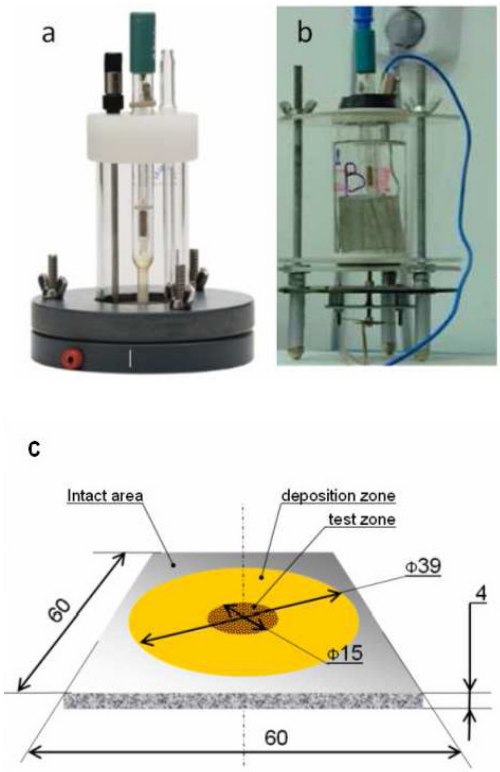

Fig. 1. Photographs of the deposition cell (a), test cell (b) and illustration of the coated and tested metallic sample (c).

curves cause irreversible damage on the electrodes. In addition, the durability of the coatings was not examined, because they are subjected to further investigations after their sealing by phosphate layer, as is proposed in [4, 29, 47, 48].

All the electrochemical procedures were performed by PG-stat Autolab 30/2, product of Ecochemie (the Netherlands). The respective impedance spectra were acquired at the following conditions: frequency range from 10^4 to 10^{-2} Hz, distributed in 7 frequencies per decade, with signal amplitude of 10 mV according to OCP. Afterwards, individual cathodic and anodic polarization curves were recorded in a larger potential interval (from OCP ± 30mV to OCP ± 500 mV, respectively), at 1 mV/s potential sweep rate. The latter curves were recorded after quenching of the polarization, caused by recording of the cathodic curves.

Superficial morphology and coating composition

The SEM observations were performed by TESCAN, SEM/FIB LYRA I XMU, supported by detector BRUKER-Quantax 200 for the EDS characterisations.

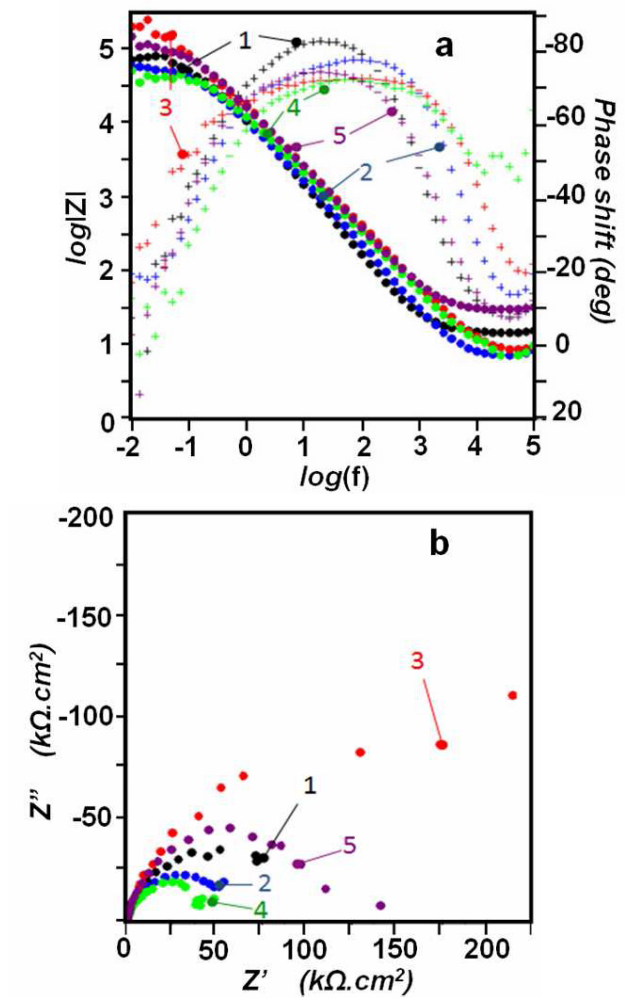

Fig. 2. EIS-spectra of samples prepared by CeCC depositions from solutions with different $(NH_4)_2Ce(NO_3)_5$ contents: 1 - 0.03M; 2 - 0.04M; 3 - 0.05M; 4 - 0.07M; 5 - 0.1M.

RESULTS AND DISCUSSION

Influence of concentration of the basic substance of the conversion bath on the features of the CeCC

Five metallic substrates were submitted to electrodeposition at -2 mA/cm², for 5 min. The concentration of the basic ingredient of the coating solution was selected to be: 0.03, 0.04, 0.05, 0.07, 0.10 M of $(NH_4)_2Ce(NO_3)_5 4H_2O$, and 10 ml. of 30 % H_2O_2 per liter of coating solution for all of them.

The barrier abilities of the respective coated specimens were examined by electrochemical measurements after 24 hours of exposition to the corrosive medium. The EIS-spectra of the samples are shown in Fig. 2.

The Bode plots of the impedance spectra look almost

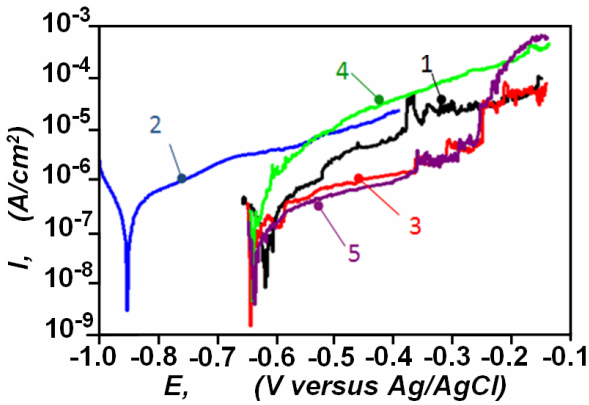

Fig. 3. Anodic polarization curves of AA2024 substrate prepared by CeCC depositions from solutions with different $(NH_4)_2Ce(NO_3)_5$ contents: 1 - 0.03M; 2 - 0.04M; 3 - 0.05M; 4 - 0.07M; 5 - 0.1M.

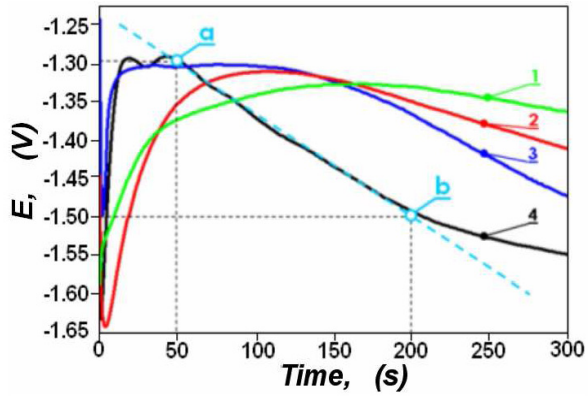

Fig. 4. Chronopotentiometric curves obtained during the galvanostatic deposition of CeCC coatings with different additions of H_2O_2 to the coating solution: 1 – 100ml/l H_2O_2; 2 - 50 – 10ml/l H_2O_2; 3 – 25ml/l H_2O_2; 4 - 10ml/l H_2O_2.

equal, whereas the Nyquist diagrams reveal remarkable differences. The largest semi-circle belongs to the sample coated in 0.05 M $(NH_4)_2Ce(NO_3)_5$ solution. Furthermore, its log|Z| - log(f) curve at 10 mHz also has the highest value, revealing that this coating possesses the best protection ability. The phase shift / log(f) curves reveal that there are two overlapped maxima, revealing presence of two, almost indistinguishable superficial layers on the substrates.

The anodic curves also partially confirm the results, obtained by EIS spectra. Fig. 3 depicts anodic curves, acquired after 24 hours of exposition to model corrosive medium of samples, coated in solutions with different $(NH_4)_2Ce(NO_3)_5$ contents.

Although the fact that the curve of the sample, prepared by 0.05 M $(NH_4)_2Ce(NO_3)_5$ deposition solution shows the best barrier ability, it also reveals clear features of pitting corrosion. The potential oscillations in -375 to -250 mV resemble the dynamic pitting nucleation/repassivation state, and the further swift rise reveals a stable pitting growth [49]. Nevertheless, the anodic current densities of this sample, (together with those, prepared by 0.1 M of the Ce-salt) stay at relatively two orders of magnitude lower than all of the rest.

Influence of oxidant addition on the features of the CeCC

The hydrogen peroxide is described as accelerator of the deposition process [50]. In order to investigate the impact of the oxidant addition, entire group of samples was submitted to CeCC deposition at equal conditions, as follows: The depositions were performed for 5 minutes at -2 mA/cm^2. The basic substance was 0.05 M in the conversion bath solution.

During the deposition at galvanostatic regime at -2 mA/cm^2, the equipment was continuously measuring the potentials versus the Ag/AgCl reference electrode and their evolution within the deposition process. The obtained potential/time diagrams are shown in Fig. 4. There, after its initial immediate fall down to almost -1.650 V, the potential reverses its values reaching about -1.300 to -1.350 V. The initial potential drop is related to the current spent for hydrogen evolution on the metallic surface. This process appears due to both of the reducing role of the cathodic current, and the generally acidic character of the deposition solution.

The subsequent reversion of the potential relays to removal of the H_2 bubbles from the metallic surface. Probably, the reason for this removal and the reversion of the potential is the so called "cathodic dissolution of the aluminium" [51, 52]. The most extended continuation is observable for the worst samples – with 100 and 50 ml/l H_2O_2 (175 s for curve 1, and 125 s for curve 2). Curves 3 and 4 of the samples with more uniform, dense and homogeneous Ce-coatings achieve maxima after 10 - 15 s.

After reaching maxima, the potentials start to drop gradually again for all curves. This phenomenon is related either to a gradual growth of uniform coatings (curves 3 and 4), or to occupation of the metallic surface by Ce-containing agglomerates. For the best coating, (10 ml/l H_2O_2), this gradual drop of potential continued

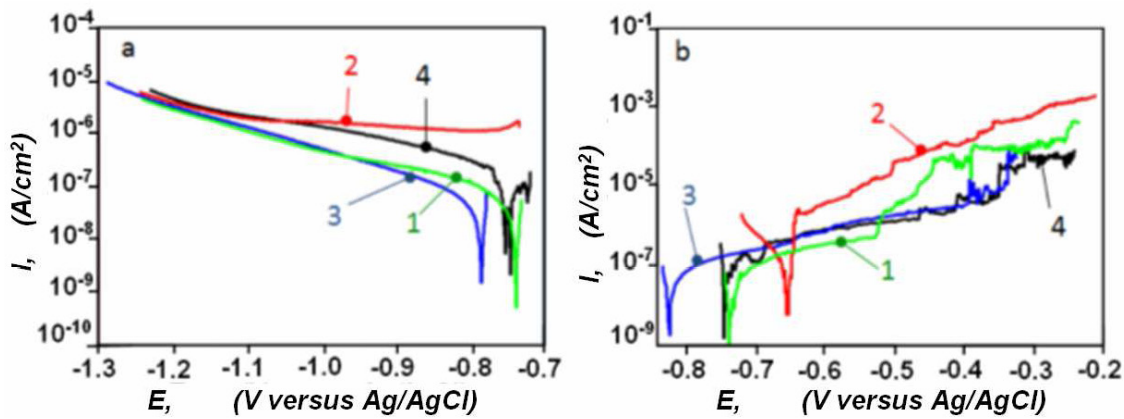

Fig. 5. Cathodic (a) and anodic (b) polarization curves recorded after 24 hours of exposition to the model corrosive medium of four specimens coated at different H_2O_2 additions: 1 – 100ml/l H_2O_2; 2 – 50 ml/l H_2O_2; 3 – 25ml/l H_2O_2; 4 - 10ml/l H_2O_2.

from the 50th (point (a)) to 200th (point (b)) second after the beginning of the deposition. During this time, the potential drops with about 200 mV. Taking into account that the deposition is performed in galvanostatic regime (-2 mA/cm^2) and applying the Ohm law, it was found that the resistance of the deposited film increases with 100 Ω cm^2 for a second. In other words, for the entire period of film growth (between points (a) and (b)) the total resistance of the best film (curve 4) raises up to 750 kΩ cm^2. Consequently, the increment of the H_2O_2 as OH^- - provider in the deposition solutions favors the dissolution of the underlying aluminum, hindering the formation of uniform and homogeneous CeCC.

Fig. 5 represents cathodic (a) and anodic (b) polarization curves recorded after 24 hours of exposition to the model corrosive medium of four specimens coated at different H_2O_2 additions.

The linear voltammogams, resemble distinguishable features of the respective specimens. All the four samples could be conditionally divided into "better" and "worse". The former have lower content of the oxidant (10 and 25 ml/l of 30% H_2O_2), whereas the latter were prepared with 50 and 100 ml/l of 30% H_2O_2 content, respectively. The anodic curve of the sample prepared by 50 ml/l. H_2O_2 shows a lack of whatever passive region. Both the cathodic and anodic curves of the sample with 100 ml/l H_2O_2 content stay at lower current densities, than those of the sample coated at 50 ml/l H_2O_2 addition. Nevertheless, the respective anodic curve (sample with 100 ml H_2O_2) has shorter region of passivity (from -750 to -550 mV vs. Ag/AgCl) than the curves of the samples with lower H_2O_2 additions. According Bethencourt et al. [53], the shorter passivity regions indicate lower strength against pitting nucleation.

Between the "better" samples, the cathodic curve of the sample prepared at 25 ml/l H_2O_2 stays at lower current densities, than this of the sample prepared at 10 ml/l content of the oxidant. However, the respective anodic curves stay at the same current densities, revealing very similar barrier ability. Furthermore, the curve of the sample with 10 ml/l oxidant addition has relatively larger passivity region (Fig. 5b, curve 4). From these relatively equivocal features of the polarization curves, it can be concluded that the optimal addition of peroxide should be in the range of 10 to 25 ml of 30 % H_2O_2 for a liter of conversion bath.

Influence of deposition current on the features of the CeCC

For investigation of the influence of the current applied, electrodepositions at -5 mA/cm^2 were performed on other set of specimens. The rest conditions were as described in the previous section (alkaline etching of the substrates, 0.05 M $(NH_4)_2Ce(NO_3)_5$ and 10, 25, 50 and 100 ml/l H_2O_2). In that manner, the coatings obtained by these conditions could be compared with the previous ones (e.g. prepared at - 2 mA/cm^2).

As could be seen from Fig. 6, the curves obtained during the electrodeposition at -5 mA/cm^2 do not possess the indicative slope for deposition of uniform, homogeneous layer described in the previous section.

The barrier abilities of the respective samples were additionally evaluated by electrochemical measurements

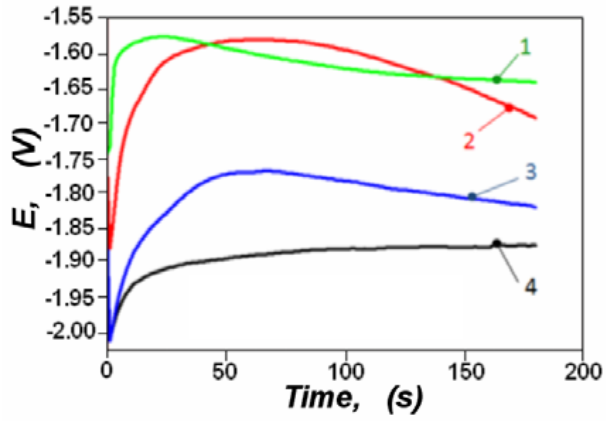

Fig. 6. Chronopotentiometric curves obtained during galvanostatic deposition of CeCC at - 5 mA/cm^2 and different additions of H_2O_2 to the coatins solution: 1 – 100 ml/l H_2O_2; 2 - 50 ml/l H_2O_2; 3 – 25 ml/l H_2O_2; 4 - 10 ml/l H_2O_2.

after 24 hours of exposition to the model corrosive medium, as well. Fig. 7 shows EIS – spectra of the samples with films deposited at - 5 mA/cm^2.

Any significant differences among the shapes of the spectra were not registered in the respective Bode plots. However, when the Nyquist plots are compared, clear differences among the radia of the respective spectra is observable. The coating, prepared at 25 ml/l of H_2O_2 obviously excels the rest two, being almost identical to those of the sample, prepared at lower oxidant content and current density. The similarity between the spectra of the specimens, prepared at -2 mA/cm^2 and 10 ml/l. of H_2O_2 (Fig. 2b, curve 3) and at -5 mA/cm^2 and 25 ml/l. H_2O_2 (Fig. 7b, curve 2) reveal compensation between the reductive effect of the cathodic current applied during the deposition, and the addition of H_2O_2 as an oxidant. In other words, at 0.05 M concentration of the cerium compound, in both cases, identical coatings could be obtained. The former approach of lower current and oxidant addition is preferable by economic point of view. Indeed, the visual inspection of the coatings obtained at the higher deposition current proved formation of rather less uniform deposits. The samples revealed rough and grain-formed agglomerates, when the higher current was used. The unsatisfying homogeneity of the coatings favors the access of corrosive species to the metallic surface, resulting in appearance of Warburg impedance tails [54] (Fig. 7b, curves 2 and 3). Curve 1 in the same figure does not possess such a tail and its radius is slightly larger than this of curve 3. Both these features of the former curve are indications of hampered corrosion products inside the defects of the coating, causing obstruction for the access of corrosive species to the substrate surface. The relation between the presence of corrosion products and the change of the shape of the EIS spectra is described elsewhere [55, 56].

Fig. 8 reveals that there are lower differences among the polarization curves of the samples prepared with different H_2O_2 additions, compared to those in Fig. 5.

This phenomenon could be easily explained, because the deposition current plays a role of reducer. As a result,

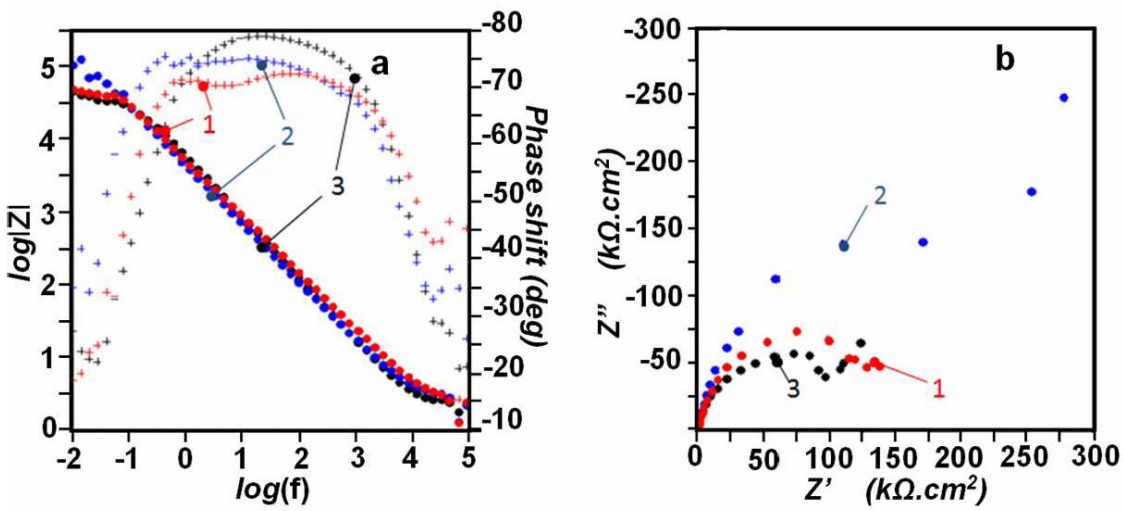

Fig. 7. Electrochemical impedance spectra, acquired after 24 hours of exposition to the model corrosive medium of four specimens coated at -5 mA/cm^2 at different H_2O_2 addition: a – Bode plot; b-Nyquist plot 1 - 50 ml/l H_2O_2; 2 – 25ml/l H_2O_2; 3 - 10ml/l H_2O_2

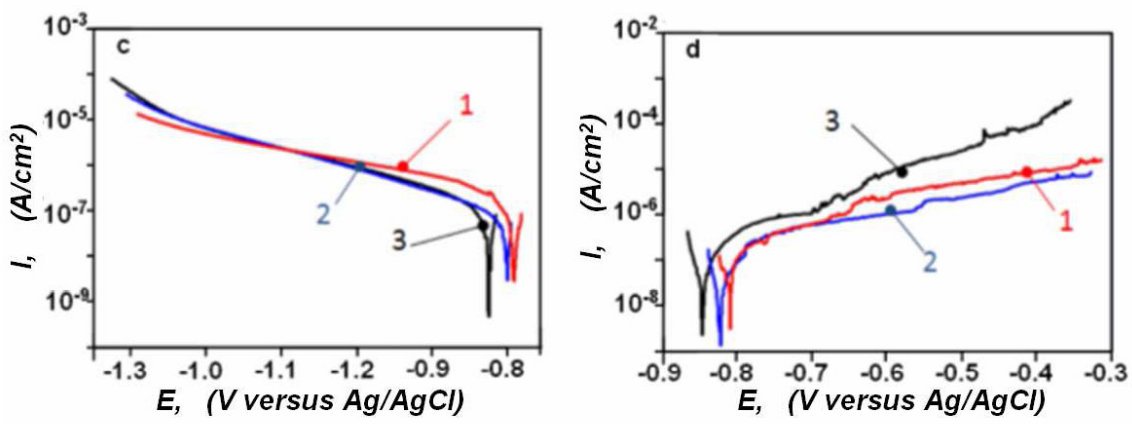

Fig. 8. Cathodic (a) and anodic (b) polarization curves recorded after 24 hours of exposition to the model corrosive medium of four specimens coated at different H_2O_2 additions: 1 - 50 ml/l H_2O_2; 2 – 25ml/l H_2O_2; 3 - 10ml/l H_2O_2.

at higher current densities (- 5 mA/cm^2), the influence of the H_2O_2 as oxidant is less notable. The supply of electrons towards the specimen (by the electric current) leads to deactivation of the peroxide by obtaining of OH^- ions [3] and acceleration of oxygen reduction. Both these processes result in supplemental alkalisation of the medium near the substrate surface and acceleration of Ce-precipitation [3, 57]. However, the obtained $Ce(OH)_3/Ce(OH)_4$ precipitates do not form any coating layer, but rather conjunction of clusters. The acceleration of the deposition process at higher current (e.g. - 5 mA/cm^2) disturbs the gradual growth of dense crystalline structures, promoting formation of agglomerates, similar to the described in previous works [58].

Morphological observations

To follow how the surfaces of the metallic specimens change after CeCC electrodeposition, and what is the level of coverage by the coatings, several SEM observations combined by EDX elemental analyses were performed. The SEM photographs (Fig. 9, positions a, c,) reveal that the entire surface is covered by the CeCC. In addition, larger oval hills are clearly distinguishable on the surface. Probably these oval hills are formed as

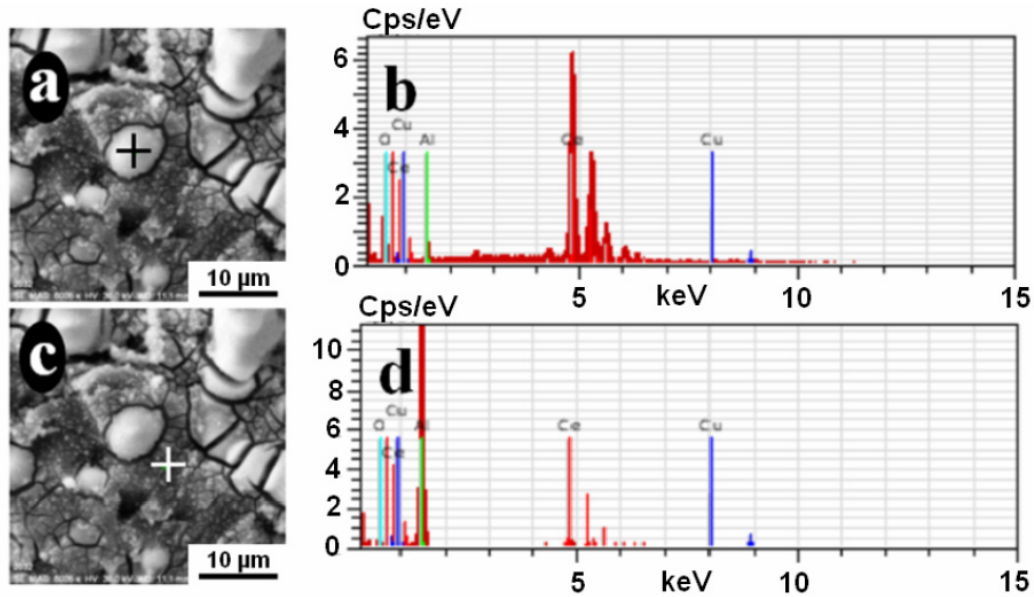

Fig. 9. SEM images (a, c) and EDX point analyses (b, d) of bright and dark zones of CeCC deposited from 0.05 M $(NH_4)_2Ce(NO_3)_5$ with 10ml/l H_2O_2 at -2 mA/cm^2

Table 2. Elemental composition determined by the point analysis of the bright and dark zone points of the coating

	El	AN	Series	unn. C [wt.%]	norm. C [wt.%]	Atom. C [at.%]	Error [%]
Bright zone	O	8	K-series	30.72	32.61	76.55	4.4
	Ce	58	L-series	58.42	62.00	16.62	1.6
	Al	13	K-series	4.28	4.54	6.32	0.3
	Cu	29	K-series	0.81	0.86	0.51	0.1
	Total:			94.23	100.00	100.00	
Dark zone	El	AN	Series	unn. C [wt.%]	norm. C [wt.%]	Atom. C [at.%]	Error [%]
	Al	13	K-series	61.53	69.61	62.54	3.1
	O	8	K-series	21.15	23.93	36.26	3.2
	Ce	58	L-series	5.40	6.11	1.06	0.2
	Cu	29	K-series	0.31	0.36	0.14	0.0
	Total:			88.39	100.00	100.00	

consequence of preferential deposition on the locations of the intermetallics, as was observed in [22].

In order to clarify the real composition of the samples and the distribution of the elements on their surfaces, EDX – point analyses were executed during the SEM observations. The elemental distributions of the most important chemical elements: Al, Ce, Cu, and oxygen were monitored. These elements were selected because the aluminium could be presented not only from the metallic substrate, but also to compose corrosion products, in form of $Al(OH)_3$, etc. The cerium was selected because this element together with the oxygen are the basic components of the coating. The copper was also selected to be monitored, because it should reveal whether the S-phase intermetalics are preferable locations of deposition, and is there a copper re-deposition as evidence of corrosion during the deposition. In order to clarify the compositions of the bright and dark zones, quantitative point analyses were performed on them. Fig. 9 shows two point analyses on a bright (position c) and dark (position d) areas of a CeCC coating, electrodeposited from 0.05 M $(NH_4)_2Ce(NO_3)_5$ with 10ml/l. H_2O_2 at -2 mA/cm^2.

After the execution of these analyses it was concluded that the bright areas are almost completely composed by Ce-oxides/hydroxides, whereas in the darker zones the Ce-content is much lower. This fact reveals that either the coating in these zones is covered or mixed with Al-containing corrosion products, or it is thin enough to allow detection of the substrate material. The latter case is possible because the depth of focus is higher than the CeCC thickness [59]. Table 2 summarizes the content of the monitored elements in the bright (Fig. 9a) and dark (Fig. 9b) zones of the specimen.

As could be seen in Table 2, that the atomic concentration Ce is almost three times higher than this of the aluminium. Surprisingly, there is unexpectedly low content of copper. This fact reveals that the superficial intermetallics are completely covered by rather thick Ce-layer. In the dark zone, more than 62 atomic units belong to Al, and only traces of Ce are represented, as can be seen in Table 2.

Comparing the tabular data for the dark and bright zones, it could be concluded that the coatings are not enough homogeneous, but they are rather represented by mixture of Ce-oxides/hydroxides, surrounded by Al-corrosion products deposited on the coating, or involved

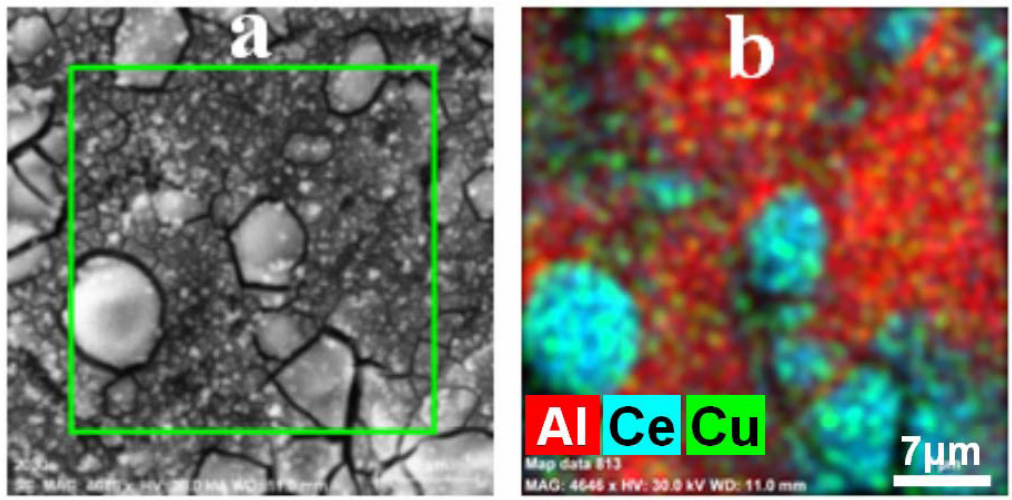

Fig. 10. EDX map data of CeCC deposited at 0.05 M $(NH_4)_2Ce(NO_3)_5$ with 10ml/l H_2O_2 at -2 mA/cm^2.

inside the CeCC-layer. Indeed, the map analysis (Fig. 10) reveals that the difference of the compositions, registered by the point analysis (Fig. 9) evinces that the Al-presence is a result of involution of corrosion products in the coating structure.

In addition, clear features of uniform copper re-deposition, as a result of the CeCC deposition procedures and/or preliminary treatment are observable in Fig. 10. This phenomenon is well described in the literature [57, 60, 61].

CONCLUSIONS

The CeCC depositions and the subsequent complex elucidation of the data obtained by the electrochemical and morphological studies provided the following conclusions:

For the investigated concentration range, from 0.03 to 0.1 M $(NH_4)_2Ce(NO_3)_5$, the optimal concentration is about 0.05 M. The optimal content of peroxide was determined to be in the range of 10 and 25 ml of 30 % H_2O_2 for liter of deposition solution.

It is established that the application of the lower current e.g. - 2 mA/cm^2 is preferable for deposition of dense and uniform coatings. The higher current density promoted formation of friable agglomerates.

Compensation was registered between the detrimental effects of the higher H_2O_2 content and the stronger current applied. The coating, deposited at -5mA/cm^2 at 25 ml/l of H_2O_2 was almost identical to those, deposited at - 2 mA/cm^2 and 10ml/l of H_2O_2 content.

By the chronopotentiometrical measurements during the deposition it was concluded that the efficient duration of the deposition of the optimal coating is about 200 seconds, any further continuation should not affect the coating characteristics, being just time wasting.

The complete coverage by the coating observed by SEM evinced that the application of cathodic currents results in the uniformity of the CeCC obtained.

Akcnowledgements

The authors gratefully acknowledge the financial support of project BG 051PO001-3.3.06-0038. Dr. G. Pelaez Lourido is acknowledged for the opportunity for the international collaboration activities.

REFERENCES

1. E. A. Starke, Jr., and J. T. Staley, Application of Modern Aluminum. Alloys to Aircraft, Prog. Aerospace Sci., 32, 1996, 131-172.
2. AIRBUS A380, Airplane characteristics, Issue 30.03.05 (2005), www.content.airbusworld.com/SITES/Technical.../AC_A380.pdf
3. M. J. O'Keefe, S. Geng, S. Joshi, Cerium-Based Conversion Coatings as Alternatives to Hex Chrome; Rare-earth compounds as providers resistance against corrosion for aluminum alloys in military applications, Metalfinishing, 2007, 25 – 28.
4. S. Geng, S. Joshi, W. Pinc, W.G. Fahrenholtz,(1)M.J. O'Keefe, T.J. O'Keefe, P. Yu, Influence of processing parameters on cerium based conversion coatings, Proceed "TRI – Service – 2007" - corrosion conference, accessible via: https://www.corrdefense.org/Technical%20Papers/Influence%20of%20Processing%20Parameters%20on%20Cerium%20Based%20Conversion%20Coatings.pdf
5. B. Hindin, Corrosion protection of aluminium alloys by corrosion prevention compounds as measured by electrochemical techniques, accessible via: https://www.corrdefense.org/Academia%20Government%20and%20Industry/XVIII%20-%20HINDIN%20-%20Corrosion%20Protection%20of%20Aluminum%20Alloys%20by.pdf
6. P. Ostash, I. M. Andreiko, Yu. V. Holovatyuk, O. I. Semenets, Effect of corrosive media on the fatigue life of degraded D16- and V95-type aluminum alloys, Mater. Sci., 44, 2008, 672 – 682.
7. J. A. Rodríguez-Martínez, A. Rusinek, A. Arias, Thermo-Viscoplastic behaviour of AA2024 aluminium sheets subjected to low velocity perforation at different temperatures, accessible via:
http://e-archivo.uc3m.es/bitstream/10016/11941/1/rodriguez_thermoTWS2011ps.pdf
8. Y. Komatsu, New Pretreatment and Painting Technology for All Aluminum Automotive Body, paper no. 910787, SAE Technical Paper Series-International Congress/ AIRP Meeting (Warrendale, PA: SAE International, 1991).
9. http://www.sbfships.com.au/
10. http://www.aluminiumleader.com/en/around/transport/ship

11. http://www.advancedrobotic.com/blog/cnc-routers/cost-savings-in-the-manufacture-of-aluminium-ships
12. D. Eyres, "Ship construction", 6th ed. 2007, Linacre House, pp. 50–52, ISBN 10:0-75-068070-9
13. http://nation.time.com/2011/07/05/u-s-navys-brand-new-aluminum-ship-foiled-by-seawater/
14. M. L. Zheludkevich, I.M. Salvado M.G. Ferreira, Sol-gel coatings for corrosion protection of metals, J. Mater. Chem., 15, 2005, 5099 - 5111.
15. G. Tsaneva, V. Kozhukharov, S. Kozhukharova, M. Ivanova, J. Gerwann, M. Schem, T. Schmidt, Functional nanocomposite coatings for corrosion protection of aluminium alloy and steel, J. Univ. Chem. Technol. Met. (Sofia), 43, 2, 2008, 231 – 238.
16. S. A. Kulinich, A. S. Akhtar, On Conversion Coating Treatments to Replace Chromating for Al Alloys: Recent Developments and Possible Future Directions, Russian Jour. Non-Ferrous Met., 53, 2012, 176-203.
17. D. Balgude, A. Sabnis, Sol–gel derived hybrid coatings as an environment friendly surface treatment for corrosion protection of metals and their alloys, J. Sol-Gel Sci. Technol. DOI 10.1007/s10971-012-2838-z
18. Directive 2004/107/EC of the European Parliament and of the Council of 15 December 2004 relating to arsenic, cadmium, mercury, nickel and polycyclic aromatic hydrocarbons in ambient air. Official Journal of the European Communities L 23, 26.1.2005, p. 3–16, Special edition in Bulgarian: Chapter 15 Volume 13 P. 124-137.
19. EU Directive 2002/95/EC "Restriction of Hazardous Substances in Electrical and Electronic Equipment" (RoHS directive 2002), www.broadcom.com/docs/ и www.chem.agilent.com/
20. U.S. Department of Health and Human Services, Public Health Service, Agency of Toxic Substances and Disease Registry (2008) Toxicological profile for Chromium, www.atsdr.cdc.gov/toxprofiles/tp7.pdf.
21. U.S. Environmental Protection Agency Washington, DC, August (1998) Toxicological review of hexavalent chromium. http://www.epa.gov/iris/toxreviews/0144tr.pdf
22. J. E. Pernas, S. Kozhukharov, E. Matter, A.A. Salve, M. Machkova, Influence of the oxidation state of Ce-ions on the inhibition of AA2024 alloy corrosion in a model corrosive medium, J. Univ. Chem. Technol. Met. (Sofia), 47, 3, 2012, 311 - 318.
23. E.A. Matter, S. Kozhukharov, M. Machkova, V. Kozhukharov, Electrochemical studies on the corrosion inhibition of AA2024 aluminium alloy by rare earth ammonium nitrates in 3.5 % NaCl solutions, Mater. Corros., 63, 2012, 1-7; DOI: 10.1002/maco.201106349
24. E. A. Matter, S. Kozhukharov, M. Machkova, V. Kozhukharov, Comparison between the inhibition efficiencies of Ce(III) and Ce(IV) ammonium nitrates against corrosion of AA2024 aluminum alloy in solutions of low chloride concentration, Corr. Sci., 62, 2012, 22 - 33.
25. M. Machkova, E. A. Matter, S. Kozhukharov, V. Kozhukharov, Effect of the anionic part of various Ce(III) salts on the corrosion inhibition efficiency of AA2024 aluminium alloy, Corr. Sci., 69, 2013, 396-405.
26. A. de Frutos, M. A. Arenas, Y. Liu, P. Skeldon, G.E. Thompson, J. de Damborenea, A. Conde, Influence of pre-treatments in cerium conversion treatment of AA2024-T3 and 7075-T6 alloys, Surf. Coat. Technol. 202, 2008, 3797-3807.
27. A. Pardo, S. Feliu, M. C. Merino, R. Arrabal, E. Matykina, The effect of cerium and lanthanum surface treatments on early stages of oxidation of A361 aluminium alloy at high temperature, Appl. Surf. Sci., 254, 2, 2007, 586-595.
28. E. Stoyanova, R. Andreeva, D. Guergova, D. Stoychev, Formation of cerium-containing conversion coatings on aluminium and its alloys as alternative to chromate (Cr^{6+}) conversion coatings, accessible via: http://mech-ing.com/journal/Archive/2011/8/95_Dimitar%20Stoichev.pdf
29. D. K. Heller, W. G. Fahrenholtz, M. J. O'Keefe, The effect of post-treatment time and temperature on cerium-based conversion coatings on Al 2024-T3, Corros. Sci., 52, 2010, 360-368.
30. B. F. Rivera, B. Y. Johnson, M.O'Keefe, W.G. Farenholz, Deposition and characterization of cerium oxide conversion coatings on aluminum alloy 7075-T6, Surf. Coat. Technol., 176, 2004, 349-356.
31. M. A. Arenas, J. J. de Damborenea, Generación de capas de conversión con elementos de tierras raras sobre acero galvanizado Rev. Metal, Extr.-Vol., 2005, 433-437.
32. L.E.M. Palomino, I.V. Aoki, H.G. de Melo, Microstructural and electrochemical characterization of Ce conversion layers formed on Al alloy 2024-T3 covered with Cu-rich smut, Electrochim. Acta, 51, 2006, 5943

– 5953.

33. A. Conde, M. A. Arenas, A. de Frutos, J. de Damborenea, Effective corrosion protection of 8090 alloy by cerium conversion coatings, Electrochim. Acta, 53, 2008, 7760-7768.
34. W. Pinc, S . Geng, M. O'Keefe, W. Fahrenholtz, T. O'Keefe, Effects of acid and alkaline based surface preparations on spray deposited cerium based conversion coatings on Al 2024-T3, Appl. Surf. Sci, 255, 2009, 4061-4065.
35. K. Brunelli, F. Bisaglia, J. Kovac, M. Magrini, M. Dabala, Effects of cathodic electrodeposition parameters of cerium oxide film on the corrosion resistance of the 2024 Al alloy, Mater. Corros., 60, 7, 2009, 514 - 520.
36. B. Jegdic, L. Živcovic, J. Popic, J. Bajat, V. MiŠkovic-Stankovic, Electrochemical methods for corrosion testing of Ce-based coating prepared on AA6060 alloy by dip immersion method, J. Serb. Chem. Soc., 78, 2013, 1-21.
37. D. Guergova, E. Stoyanova, D. Stoychev, I. Avramova, G. Atanasova, P. Stefanov, Corrosion stability of stainless steel, modified electrochemically with Ce_2O_3–CeO_2 films, in 3.5% NaCl media, Bulgarian Chem. Commun. 43, 1, 2011, 150-157.
38. D. Nickolova, E. Stoyanova, D. Stoychev, I. Avramova, P. Stefanov, Protective effect of alumina and ceria oxide layers electrodeposited on stainless steel in sulfuric acid media, Surf. Coat. Technol., 202, 2008, 1876-1888.
39. E. Stoyanova, D. Guergova, D. Stoychev, I. Avramova, P. Stefanov, Passivity of OC 404 steel modified electrochemically with CeO_2-Ce_2O_3 oxide layers in sulfuric acid media, Electrochim. Acta 55, 2010, 1725 - 1732.
40. D. Guergova, E. Stoyanova, D. Stoychev, G. Atanasova, I. Avramova, P. Stefanov. Influence of calcination of SSOC 4004 with alumina or ceria layers on their passive state in different acid media. Bulgarian Chem. Commun., 40, 2008, 227-232.
41. H. Hasannejad, M. Aliofkhazraei, A. Shanaghi, T. Shahrabi, A. R. Sabour, Nanostructural and electrochemical characteristics of cerium oxide thin films deposited on AA5083-H321 aluminum alloy substrates by dip immersion and sol-gel methods, Thin Solid Films, 517, 17, 2009, 4792-4799.
42. accessible via: http://www.splav.kharkov.com/en/e_mat_start.php?name_id=1438
43. accessible via: http://www.metalsnab.com/en/news/iso_cert.php
44. J. Vogelsang, The new standards for EIS measurements on coatings. Short course on EIS, proceeds. 6–7 November, 2008, Lisbon (Portugal).
45. M. Machkova, E. A. Matter, S. Kozhukharov, V. Kozhukharov, Effect of the anionic part of various Ce(III) salts on the corrosion inhibition efficiency of AA2024 aluminium alloy, Corr. Sci. 69, 2013, 396 – 405.
46. E. A. Matter, S. V. Kozhukharov, M. S. Machkova, Effect of preliminary treatment on the superficial morphology and the corrosion behaviour of AA2024 aluminum alloy, Bulgarian Chem. Comm., 43, 1, 2011, 23-30.
47. D. K. Heller, W. G. Fahrenholtz, M. J. O'Keefe Effect of Phosphate Source on Post-Treatment of Cerium-Based Conversion Coatings on Al 2024-T3, J. Electrochem. Soc., 156, 11, 2009, C400-C406.
48. H. Zhang, Y. Zuo, The improvement of corrosion resistance of Ce conversion films on aluminum alloy by phosphate post-treatment, Appl. Surf. Sci., 254, 2008, 4930-4935.
49. K. Srinivasa Rao, K. Prasad Rao, Pitting Corrosion of heat-treatable aluminium alloys and welds: a review, Trans Indian Inst. Met., 57, 2004, 593-610.
50. F.H. Scholes, C. Soste, A. E. Huges S. G. Hardin, P. R. Curtis, The role of hydrogen peroxide in the deposition of cerium-based conversion coatings, Appl. Surf. Sci., 253, 2006, 1770-1780.
51. M. Mokaddem, P. Volovitch, F. Rechou, R. Oltra, K. Ogle, The anodic and cathodic dissolution of Al and Al-Cu-Mg alloy, Electrochim. Acta, 55, 2010, 3779 -3786.
52. K. Ogle, M. Serdechnova, M. Mokaddem, P. Volovitch, The cathodic dissolution of Al, Al_2Cu, and Al alloys, Electrochim. Acta, 56, 2011, 1711 – 1718.
53. M. Bethencourt, F.J. Botana, M.J. Cano, M. Marcos, J.M. Sánchez-Amaya, L. González-Rovira, Behaviour of the alloy AA2017 in aqueous solutions of NaCl. Part I: Corrosion mechanisms, Corros. Sci. 51, 2009, 518-524.
54. M. Garcia-Heraz, A. Jimenez-Moralez, B. Casal, J. Galvan, S. Radzki, A.Villegas, Preparation and electrochemical study of cerium-silica sol-gel films, J. Alloys Compd 380, 2004, 219 - 224.
55. A. A. Salve, S. Kozhukharov, J.E. Pernas, E. Matter, M. Machkova, A comaparive research on hybrid and hybrid nano-composite protective primary coatings for

AA2024 aircraft alloy, J. Univ. Chem. Technol. Met. (Sofia), 47, 3, 2012, 319-326.

56. S. Kozhukharov, V. Kozhukharov, M. Schem, M. Aslan, M. Wittmar, A. Wittmar, M. Veith, Protective ability of hybrid nano-composite coatings with cerium sulphate as inhibitor against corrosion of AA2024 aluminium alloy, Prog. Org. Coat., 73, 2012, 95-103.
57. K. A. Yasakau, M. L. Zheludkevich, S. V. Lamaka and M. G. S, Ferreira, Mechanism of Corrosion Inhibition of AA2024 by Rare-Earth Compounds, J. Phys. Chem. B, 110, 2006, 5515-5528.
58. E. Matter, S. Kozhukharov, M. Machkova, SEM & EDS determination of the impact of inhibitor containing corrosive media over the AA2024 superficial morphology, Ann. Proceeds. "Angel Kanchev" University of Rousse (Bulgaria), 50, 9.1, 2011, 60-64.
59. P. E. López, J-B. Carda Castelló, E. C. Cordoncillo, Esmaltes y Pigmentos Ceramicos, Faenza Edirtice Iberica, S. L. Catellon (Spain) 2001, pp. 287-300.
60. M. Bethencourt, F.J. Botana, J.J. Calvino, M. Marcos, M.A. Rodriguez-Chacón, Lanthanide compounds as environmentally-friendly corrosion inhibitors of aluminium alloys: a review, Corros. Sci., 40, 1998, 1803-1819.
61. Y. Liu, M.A. Arenas, S.J. Garcia-Vergara, T. Hashimoto, P. Skeldon, G.E.Thompson, H. Habazaki, P. Bailey, T.C.Q. Noakes, Behaviour of copper during alkaline corrosion of Al-Cu alloys, Corros. Sci., 50, 2008, 1475-1480.